ON IMPROVING THE ACCURACY OF T1 MAPPING OF THE HUMAN BRAIN

Yung-Yeh Chang[1], Kenneth A. Kraft[2], and Alen Docef[1]

[1]Department of Electrical and Computer Engineering, Virginia Commonwealth University
601 West Main Street, Richmond, Virginia, 23284, USA
phone: + (1) 804-827-7032, fax: + (1) 804-827-0006, email: {changy2,adocef}@vcu.edu
web: www.egr.vcu.edu
[2]Department of Radiology, Virginia Commonwealth University
1101 East Marshall Street, Richmond, Virginia, 23298, USA
phone: + (1) 804-828-4238, fax: + (1) 804-828-6129, email: kakraft@vcu.edu
web: www.radiology.vcu.edu

ABSTRACT

The focus of the presented research is to improve the accuracy in T_1 mapping of the human brain using magnetic resonance imaging (MRI). Quantitative T_1 imaging is essential for the non-invasive detection and characterization of brain edema. Existing techniques are either very slow or provide inadequate accuracy. A method for improving the accuracy of the Inversion Recovery Fast Spin Echo MRI sequence is investigated. The approach is based on matching the image reconstruction algorithm to the noise present in the magnetic resonance echo signal measurements. A reduction in T_1 estimation error by 36% is achieved.

1. INTRODUCTION

Magnetic Resonance (MR) imaging is one of the most widely used imaging modalities, with applications ranging from well-established diagnostic studies to cutting-edge image-guided brain surgery [2]. One clinical application of MR imaging is the non-invasive detection and characterization of brain edemas resulting from head trauma or pathological conditions. This is accomplished by measuring the water content at different anatomical locations, resulting in a water map of the brain. MR imaging is well suited for this process due to its inherent sensitivity to changes in water content. It has been shown [8] that a linear relation exists between the inverse of the water content W and the inverse of the longitudinal nuclear magnetic relaxation time T_1. For a fixed magnetic field strength, the relationship

$$\frac{1}{W} = A + \frac{B}{T_1} \qquad (1)$$

allows the water map to be determined from a T_1 map. This method has been validated experimentally for water content measurements in phantoms and cat brains [8] and in the human brain [9].

Conventional MR imaging routinely being used in various diagnostic scenarios produces T_1- or T_2-weighted images, which are qualitative images that reasonably preserve anatomic detail but cannot estimate T_1 (or T_2) accurately. Accurate quantitative T_1 mapping is customarily realized using inversion recovery (IR) combined with Fast Spin Echo (FSE) imaging. A shortcoming of T_1 mapping using inversion recovery is that it results in a very long scan time, mostly because of the considerable waiting time between the inversion and excitation pulses which, for accurate T_1 measurements, can be up to 1900 ms [9]. Consequently, a conventional IR spin echo sequence can last 35 minutes per slice [14].

Fast acquisition is essential for any imaging modality in order to avoid motion artifacts. Several approaches have been employed to address the issue of motion artifacts, such as respiratory gating, cardiac triggering, BLADE/Propeller MR sequences [12], Prospective Acquisition Correction (PACE) sequences [13], and Integrated Parallel Acquisition Techniques (iPAT) [7]. However, they do not reduce the scan time. They could be used in conjunction with a fast T_1 mapping method to prevent patient discomfort and increase patient throughput.

A fast T_1 mapping technique was developed by Clare and Jezzard [5] by combining single-shot gradient Echo Planar Imaging (EPI) with multi-slice inversion recovery. To achieve different inversion times TI for each pixel in each slice in a time-efficient fashion, the volume is scanned several times, each time with a different slice ordering scheme. EPI is one of the fastest imaging methods available, so it is not surprising that Clare and Jezzard's method is very fast: it acquires 60 slices covering the entire brain with 3 minutes. However, it does this by using a lower spatial resolution (128 by 128 pixels, 256 mm by 256 mm). The T_1 values are estimated with good reproducibility (error no larger than 5%) but the accuracy of this method has not been proven. In fact, the paper only reports reproducibility, but it is known that the EPI method lacks in accuracy. To improve on the accuracy of T_1 mapping, Zhu and Penn [14] extended the multislice method with variable slice ordering to Inversion Recovery FSE. Spin echo imaging is affected much less by magnetic field inhomogeneity compared to gradient echo imaging, resulting in more accurate T_1 measurements. Zhu and Penn's method collects 2 sets of 12 slices in 13 minutes. It uses a still somewhat low spatial resolution (256 by 128 pixels, 280 mm by 280 mm). The maximum RMS error is 5.24%. This method is more accurate but has a longer scan time.

We believe that further reductions in scan time without a decrease in spatial resolution will involve trade-offs between speed and accuracy. Therefore, in this paper we focus on improving the accuracy of Inversion Recovery FSE in order to provide the best starting point for the speed-accuracy optimization. To give the reader a rough measure of the target accuracy, we point out that, to determine water content with an absolute precision of $\Delta W = 0.01$, the relaxation T_1 must be computed with a relative precision of $\Delta T_1/T_1 = 0.04$ [8].

This paper is organized as follows. In Section 2 the T_1 mapping algorithm is introduced. The experimental setup is described in Section 3. T_1 estimation performance results are presented and discussed in Section 4. Concluding remarks are given in Section 5.

2. THE T_1 ESTIMATION METHOD

The goal of our research has been to improve the accuracy of Zhu and Penn's T_1 mapping method. Therefore, a brief description of the method is necessary. In IR-FSE, a 180° *inversion* RF pulse is first applied to rotate the net magnetization in the negative direction of the z axis. As the tissue returns to the equilibrium position along the positive z axis with spin-lattice (T_1) relaxation time, a 90° *excitation* RF pulse is applied to rotate the longitudinal magnetization into the x-y plane. Finally, a 180° *refocusing* pulse is applied to refocus the magnetic spins in order to generate signal echoes which can be acquired. The *inversion time* TI, the wait time between the first and second RF pulse, is the main cause of the long IR scan time. Furthermore, accurate measurement of T_1 requires repeating the IR-FSE sequence multiple times, with different inversion times TI.

The echo signal for this sequence is given by the equation [14]

$$S = M\left(\left(1 - e^{-TI/T_1}\right) - f_{inv}\left(1 - e^{-T_{SPIR}/T_1}\right)e^{-TI/T_1}\right) \quad (2)$$

Here M is a quantity depending of the longitudinal magnetization at equilibrium, the time of echo TE, the transverse relaxation time T_2, and a gain factor dependent on the transmitter and receiver. TI is the inversion time and f_{inv} is the effective spin inversion fraction which models the fact that not all spins are inverted by exactly 180°. T_{SPIR} is a constant time parameter of the sequence.

The relaxation time T_1 is determined using a curve fitting approach. For each pixel in the field of view, several measurements (S_i) are taken for different values of the inversion time (TI_i). Then the curve defined by Equation (2) is fitted to the measurement data (TI_i, S_i) by choosing the right parameters (T_1, M and f_{inv}). Since there are three parameters, at least three measurements S_i must be taken. While only three measurements have indeed been used (for example, in [4]), more commonly five or six measurements are taken, for inversion times in the range of 150 ms to 1900 ms. This is done in order to obtain more robust T_1 estimates from noisy measurements.

The curve parameters (T_1, M, f_{inv}) are obtained by numerical optimization of a cost function J(T_1, M and f_{inv}) that quantifies the discrepancy between the signal values modelled by Equation (2) and the actual signal measurements:

$$J(T_1, M, f_{inv}) = \sum_{i=1}^{N-1} \left| S(T_1, M, f_{inv}, TI_i) - S_i \right| \quad (3)$$

Here the summation is taken over all measurements. When the cost function reaches a minimum, an estimate of T_1 (and also M and f_{inv}) is obtained. To simplify the optimization process, the amplitude parameter M can be eliminated by using a modified cost function that only has two parameters:

$$J(T_1, f_{inv}) = \sum_{i=1}^{N-1} \left\| \frac{S(T_1, M, f_{inv}, TI_i)}{S(T_1, M, f_{inv}, TI_N)} \right| - \left| \frac{S_i}{S_N} \right\| \quad (4)$$

By normalizing both the model term and the measurement term, the amplitude parameter M cancels out. Computational complexity is reduced and the probability of suboptimal local minima is diminished.

Zhu and Penn achieved a significant reduction in acquisition time by using a multislice method in which the inversion RF pulse inverts a group of slices and different excitation pulses excite individual slices for which spin echoes are then generated and captured. By using multiple passes over the group of slices and using a different slice ordering scheme for each pass, the IR-FSE sequence effectively packs measurements with multiple TI values in a short scan time.

Our proposed improvements to the existing T_1 mapping method follow from the experimental observation that echo signal measurements for different values of the inversion time TI are affected by noise differently. In other words, the random variables S_i consist of the echo signal and different amounts of noise. Therefore, the N measurements are not equally reliable. This observation can be exploited by giving more emphasis to more accurate signals. We achieve this goal by employing different weights in the cost function used in the curve fitting:

$$J(T_1, f_{inv}) = \sum_{i=1}^{N-1} w_i \left\| \frac{S(T_1, M, f_{inv}, TI_i)}{S(T_1, M, f_{inv}, TI_N)} \right| - \left| \frac{S_i}{S_N} \right\| \quad (5)$$

If the statistical properties of the measurement noise were known, one could attempt to find the optimal weights w_i analytically. However, a widely accepted model for the noise does not yet exist. A 1992 study [6] showed that the signal-to-noise ratio (SNR) for IR-FSE is relatively constant for cerebrospinal fluid, and decreases with the inversion time TI for grey and white matter. But the noise was studied only for small TI values (20 to 400 ms). A more recent study ([1] in Figure 3) indicates that the noise level itself (rather than the SNR) is constant with TI in IR-FSE. As shown later in this paper, our own analysis indicates that the noise level increases with TI. This suggests that, to emphasize the more reliable measurements, which are those with smaller absolute values, a reasonable choice for the weights w_i is

$$w_i = \frac{1}{|S_i|^{\alpha}}, \quad (6)$$

where α is a real number to be determined. This approach has been used, for a weighted mean-square cost function with $\alpha = 2$, by Bakker in [3], in the context of sign restoration when only the magnitude of the IR signal is available.

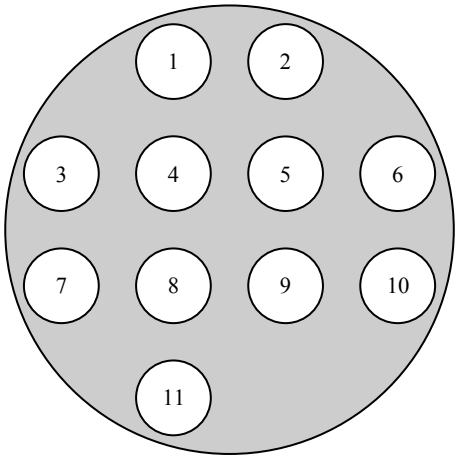

Figure 1: MRI phantom tube configuration.

Since no analytical optimization of the weights can be carried out, due to the lack of a model for measurement noise, we choose the weights according to Equation (6) and we optimize the parameter α using experimental data obtained from a phantom study, where the ground truth (true T_1) is available. The optimum value of α is determined by minimizing the T_1 estimation error over the entire image. The resulting value is to be used for subsequent clinical studies. We should point out that the optimum α is not a constant to be used for any IR-FSE sequence; it is very likely to vary when sequence parameters and scanner model are changed.

The optimum α is also likely to be different for tissues with different relaxation time T_1. Using phantom studies with simulated tissues with different T_1 values, this dependency can be tabulated. Therefore, we propose a two-pass adaptive T_1 estimation technique that attempts to exploit this variation. In a first pass, a rough T_1 map is obtained by minimizing a cost function that uses a globally optimal α. Then, for each pixel, based on the rough estimate, we choose the locally optimal α from the table obtained in the phantom studies. Finally, a refined T_1 estimate is obtained by using the locally optimal α in the cost function.

3. THE EXPERIMENTAL SETUP

To perform noise analysis and evaluate the performance of the proposed T_1 estimation method, the IR-FSE sequence has been run on a 1.5 Tesla Siemens Avanto MRI scanner with the VB17A operating system. Twelve inversion times have been used: 50, 300, 550, 800, 1050, 1300, 1550, 1800, 2050, 2300, 2550, and 2800 ms. Such a large number of inversion times is impractical in clinical T_1 mapping, but it is useful for measurement noise analysis. A large repetition time TR = 3000 ms has been chosen so that the effects due to small TR can be neglected and all measurement imperfections can be assumed to be due to noise. Each acquired image was 256 by 256 pixels, covering a field of view of 300 by 300 mm. To maintain a reasonable scan time, only two slices were acquired. The proposed method is independent of the number of slices.

To evaluate the accuracy of T_1 mapping methods, the ground truth data should be available. This is very difficult to obtain for live patients and, to our knowledge, anatomically-realistic MR phantoms are not available. Therefore, we developed a phantom made up of 11 tubes containing different gels with known T_1 and T_2 values. The tubes have been mounted in a casing, as shown in Figure 1. Each tube contains 50 mL of nickel-doped agarose gel prepared according to [10]. Some of the target T_1 values were chosen to mimic grey and white matter, some just to cover the interval of typical values encountered in T_1 brain imaging. To obtain the true T_1 values of these gels, the tubes have been measured using NMR spectroscopy. The true T_1 values are listed in the second row of Table 2.

3.1 Noise Analysis

The purpose of this analysis is to identify the relationship between the noise variance and the noise-free measurement. To this end, we started by manually segmenting the interior of each tube in the image. Each pixel is then labelled either by the tube index (1, 2, …, 12) or as background. For each tube and for each TI value, we compute the mean and standard deviation of the measurements corresponding to the pixels inside the tube. These values are interpreted as the noise-free signal and the noise standard deviation.

3.2 Estimation Using Optimum Weights

The T_1 estimation method described in Section 2 is used to obtain a T_1 map of the phantom. For numerical minimization of the cost function during T_1 estimation, the Levenberg-Marquardt algorithm [11] has been employed. The T_1 mapping process was repeated for several values of α, and each time the RMS value of the estimation error ($T_{1,est}$-$T_{1,true}$) was computed. The value of α yielding the lowest RMS error is chosen to compute the optimum weights according to Equation (6).

3.3 Estimation Using Adaptive Weights

During the weight optimization described in the previous subsection, both per-tube RMS errors and a global RMS error are recorded. For each tube, then, we can choose an optimum parameter α, that minimizes the T_1 estimation error for that tube. To evaluate the global estimation error, a second estimation pass is performed with tube-specific α values.

4. RESULTS AND DISCUSSION

4.1 Noise Analysis

The noise analysis results are provided in Table 1. For each phantom tube and for each TI value, the mean and standard deviation of the echo signal measurement are listed. It is easy to notice that the noise level is not constant: stronger noise occurs in measurements with larger absolute values. On the other hand, if the SNR is computed (the mean divided by the standard deviation), it is not constant across measurement levels, as illustrated in Figure 2 for two differ-

ent phantom tubes. So the relationship between the noise level and the measurement is not a simple one.

There is no doubt that a more in-depth analysis of measurement noise is needed, perhaps investigating the noise probability distribution function and its dependency on the IR-FSE sequence parameters. The simple analysis presented here was included only to justify the weighted optimization approach and to show that a noise model is not easy to infer from the experimental data.

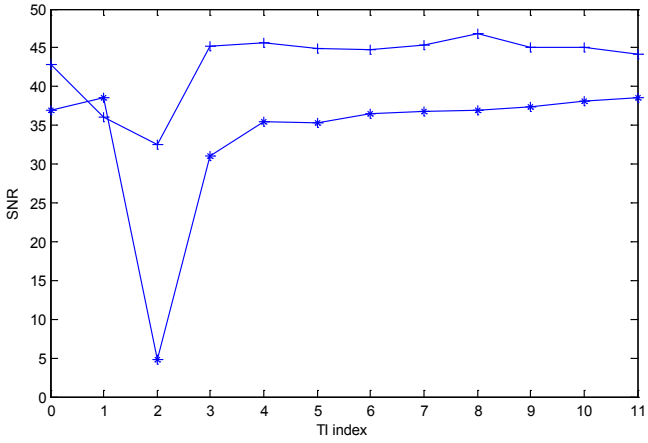

Figure 2: SNR as a function of TI index in IR-FSE.

4.2 Estimation Using Optimum Weights

The RMS T_1 estimation error values are listed in Table 2 for the 11 tubes and values of α ranging from -0.2 to +1.0. As anticipated, using different weights for the terms corresponding to different inversion times in Equation (5) leads to a reduction in estimation error for all the tubes compared to the case with no weights (α = 0). An aggregate estimation error is also computed and reported in the last column of the table. The variation of the aggregate error with α is shown in Figure 3. We observe an overall reduction in estimation error by 36% when α ≈ 0.5 is used.

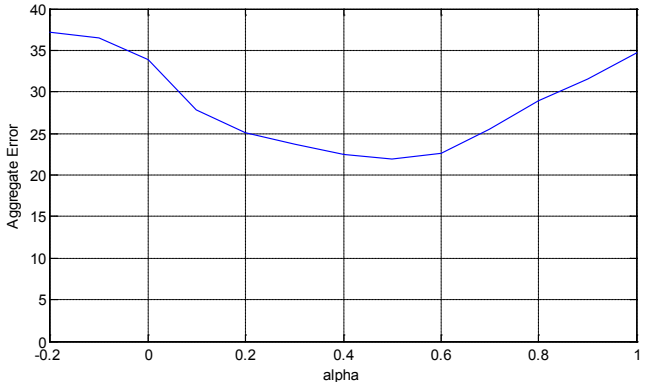

Figure 3: Aggregate estimation error as a function of α.

4.3 Estimation Using Adaptive Weights

To evaluate the two-pass adaptive estimation method described Subsection 3.3, it would be necessary to first create a robust method for determining the optimum α for a given relaxation time T_1. To evaluate the potential performance of this adaptive method, we simply use, for each tube, the optimum α obtained in the previous subsection, without worrying about the robustness of this approach. The resulting aggregate estimation error equals 20.53, which is only a bit smaller than 21.88, the error obtained for a fixed α = 0.5. So the adaptive method provides a further reduction in error of 4%. This minor further improvement does not justify the additional algorithm complexity.

A note on the computational complexity of the proposed method is necessary. Although image reconstruction is performed off-line and therefore does not have real-time constraints, it cannot last unreasonably long. The single-pass, fixed-weights method requires N-1 extra multiplications per evaluation of the cost function (Equation (5)). The weights can be pre-computed once for each pixel. The time to perform these additional computations is minor when compared to the other terms in the cost function, in particular $S(T_1, M, f_{inv}, TI_i)$. For the two-pass, adaptive-weights method, the reconstruction time can be twice as long.

5. CONCLUSION

A method for improving the accuracy of the IR-FSE sequence used in quantitative T_1 imaging of the human brain has been proposed. By employing a weighted cost function that emphasizes more reliable measurement data, a reduction in T_1 estimation error by 36% has been achieved without major computational overhead. A further 4% reduction was achieved by using a more demanding two-pass technique. A simple analysis of noise in IR-FSE has been performed and results indicate that the noise is complex in nature and difficult to model.

REFERENCES

[1] G. Andreisek, J. M. Froehlich, J. Hodler, et al. "Direct MR arthrography at 1.5 and 3.0 T: signal dependence on gadolinium and iodine concentrations--phantom study". *Radiology*. 2008 Jun;247(3):706-16.

[2] AFP. "Paris hospital hosts pioneering laser brain surgery". *France 24*, 2008, August 30. Available at http://www.france24.com/en/2080830.

[3] C. J. G. Bakker, C. N. De Graaf, P. Van Dijk. "Restoration of Signal Polarity in a Set of Inversion Recovery NMR Images". *IEEE Transactions on Medical Imaging*, 1984:3(4):197-202.

[4] C. J. G. Bakker, C. N. de Graaf, P. Van Dijk. "Calculation of Zero-Crossing and Spin-Lattice Relaxation Time Pictures in Inversion Recovery NMR Imaging". *IEEE Transactions on Biomedical Engineering*, 1985:BME-32(7):535-539.

[5] S. Clare, P. Jezzard. "Rapid T_1 mapping using multislice echo planar imaging". *Magn Reson Med* 2001:45:630-634.

[6] R. T. Constable, R. C. Smith, J. C. Gore. "Signal-to-noise and contrast in fast spin echo (FSE) and inversion recovery FSE imaging". *J Computer Assisted Tomography* 1992;16(1):41-7.

[7] O. Dietrich, K. Nikolaou, B. J. Wintersperger, et al. "iPAT: applications for fast and cardiovascular MR imaging". *Electromedica* 70:133–46, 2002.

[8] P. P. Fatouros, A. Marmarou, K. A. Kraft, et al. "In vivo brain water determination by T1 measurements: effect of total water content, hydration fraction, and field strength". *Magn Reson Med* 1991:17(2):402-413.

[9] P. P. Fatouros, A. Marmarou. "Use of magnetic resonance imaging for in vivo measurements of water content in human brain: method and normal values". *J Neurosurg* 1999:90:109-115.

[10] K. A. Kraft, P. P. Fatouros, G. D. Clarke, P. R. S. Kishore, "An MRI Phantom Material for Quantitative Relaxometry". *Magn Reson Med* 1987:5:555-562.

[11] J. J. Moré, "The Levenberg–Marquardt algorithm: implementation and theory, numerical analysis". *Lecture Notes in Mathematics*, vol 630, pp 105–116, Springer, Heidelberg, 1977.

[12] J. G. Pipe, "Motion Correction With PROPELLER MRI: Application to Head Motion and Free-Breathing Cardiac Imaging", *Magn Reson Med* 1999:42:963–969.

[13] S. Thesen, O. Heid, E. Mueller, L. R. Schad, "Prospective acquisition correction for head motion with image-based tracking for real-time fMRI", *Magn Reson Med* 2000:44(3):457-65.

[14] D. C. Zhu, R. D. Penn. "Full-brain T_1 mapping through inversion recovery fast spin echo imaging with time-efficient slice ordering". *Magn Reson Med* 2005:54:725-731.

Tube	1	2	3	4	5	6	7	8	9	10	11
TI (ms)	Mean										
50	-2358.03	-2404.86	-2541.28	-2397.67	-2400.65	-2512.83	-2664.37	-2560.34	-2526.36	-2665.48	-2594.06
300	-329.60	-677.21	-611.54	-337.05	-648.39	-1273.66	-985.77	-859.70	-937.35	-927.46	-1016.25
550	802.18	352.00	511.10	784.79	363.08	-456.29	49.34	139.59	16.59	139.16	-25.75
800	1548.94	1110.28	1313.52	1543.86	1115.05	253.30	856.90	925.17	778.29	951.46	753.41
1050	2030.52	1642.33	1865.12	2039.68	1649.67	827.46	1467.90	1509.21	1362.03	1558.52	1347.60
1300	2342.72	2021.38	2238.37	2358.92	2024.86	1291.72	1914.51	1933.34	1794.72	1992.58	1786.92
1550	2547.61	2290.34	2506.76	2575.32	2297.17	1676.18	2260.65	2255.37	2126.69	2329.72	2136.76
1800	2669.61	2475.75	2671.54	2696.51	2474.57	1980.57	2496.74	2473.66	2359.79	2550.69	2376.18
2050	2759.70	2615.27	2811.26	2795.09	2619.46	2244.08	2703.21	2659.35	2562.06	2748.98	2591.34
2300	2806.62	2706.84	2884.52	2847.81	2709.93	2442.97	2826.86	2775.13	2691.61	2858.81	2718.92
2550	2844.43	2771.64	2939.28	2875.96	2770.22	2609.12	2934.63	2865.34	2794.08	2954.23	2833.05
2800	2863.14	2819.90	2980.77	2905.45	2821.34	2751.42	3015.08	2936.48	2874.76	3030.19	2921.96
	Standard Deviation										
50	53.34	56.11	58.09	48.55	58.41	65.29	72.06	147.79	74.21	63.88	66.10
300	20.21	18.78	17.72	14.26	18.79	26.97	25.54	56.16	25.04	25.40	22.52
550	16.13	10.82	12.28	15.01	12.08	11.34	10.41	11.14	10.05	12.20	10.09
800	25.83	24.54	28.28	26.66	25.63	24.93	27.65	50.65	31.20	24.21	26.17
1050	36.71	36.03	38.98	34.95	37.88	37.51	41.38	83.08	45.50	35.96	40.67
1300	42.83	44.97	47.06	40.60	46.85	48.11	54.19	105.36	56.93	46.20	50.82
1550	48.51	51.10	52.68	45.32	53.02	54.46	61.91	126.55	63.55	52.58	58.89
1800	50.81	54.65	55.25	48.27	57.44	62.36	67.82	135.28	70.35	56.26	62.70
2050	52.28	55.89	58.49	50.13	61.32	65.32	73.14	145.46	76.85	62.10	68.28
2300	55.27	60.00	61.11	52.26	62.25	68.94	75.61	152.28	79.06	62.55	70.11
2550	54.39	61.51	62.39	53.47	63.78	73.60	76.84	158.86	79.26	64.33	69.56
2800	55.47	63.86	63.95	53.35	64.75	74.02	78.18	160.78	80.96	66.84	74.37

Table 1: Mean and standard deviation for the MR echo signal measured in the 11 tubes for different inversion times.

Tube	1	2	3	4	5	6	7	8	9	10	11	All
True T1 (ms)	576	737	682	575	734	1258	875	834	903	834	907	
$\alpha = -0.2$	18.25	29.63	30.42	11.15	27.67	68.38	39.53	35.26	42.51	40.92	34.87	37.22
$\alpha = -0.1$	18.82	30.31	30.99	11.57	28.20	60.51	40.43	36.48	43.06	41.68	35.25	36.46
$\alpha = 0.0$	19.87	30.47	31.77	11.97	28.64	53.08	36.84	33.44	39.40	39.83	30.57	33.94
$\alpha = 0.1$	19.37	23.39	28.12	12.81	21.53	50.00	27.19	24.52	29.80	30.02	23.24	27.89
$\alpha = 0.2$	13.74	18.89	22.31	10.59	16.67	47.64	25.85	22.31	27.97	27.31	21.74	25.05
$\alpha = 0.3$	9.07	17.36	19.93	11.93	15.08	46.53	24.80	21.28	26.25	25.84	20.68	23.73
$\alpha = 0.4$	8.66	15.46	15.91	13.67	13.32	45.14	23.88	19.96	25.32	24.36	19.70	22.54
$\alpha = 0.5$	8.62	13.57	10.13	13.85	11.66	44.02	23.02	18.86	26.35	22.53	22.80	21.88
$\alpha = 0.6$	8.49	10.35	7.73	13.98	8.82	43.27	23.55	18.37	32.62	22.01	27.53	22.62
$\alpha = 0.7$	7.98	10.65	7.94	13.81	8.85	44.46	29.50	20.35	40.83	23.76	33.43	25.55
$\alpha = 0.8$	8.00	12.95	8.93	13.39	11.12	49.92	33.08	23.49	46.68	25.38	39.96	28.99
$\alpha = 0.9$	9.60	21.40	14.15	16.62	17.16	56.24	29.10	24.67	46.26	28.73	44.34	31.58
$\alpha = 1.0$	13.82	25.00	29.63	20.32	24.76	66.85	21.36	27.22	41.84	30.21	45.67	34.71

Table 2: T_1 estimation error RMS values for the 11 tubes and for different values of α.